Thin Solid Films 742 (2022) 139053

Contents lists available at ScienceDirect

Thin Solid Films

journal homepage: www.elsevier.com/locate/tsf

Study of the structure and optoelectronic properties of $Cu_2Ge(Se_xS_{1-x})_3$ microcrystalline powders

X. Li *, K. Timmo, M. Grossberg, M. Pilvet, R. Kaupmees, J. Krustok, K. Muska, V. Mikli, M. Kauk-Kuusik

Department of Materials and Environmental Technology, Tallinn University of Technology, Ehitajate tee 5, Tallinn 19086, Estonia

ARTICLE INFO

Keywords:
Copper germanium sulfoselenide
Crystal structure
Photoluminescence
Raman spectroscopy
Solar cell

ABSTRACT

In this study, the $Cu_2Ge(Se_xS_{1-x})_3$ (x = 0, 0.2, 0.4, 0.6, 0.8, 1) microcrystalline powders were synthesized from elemental precursors in the liquid phase of lithium iodide (LiI) flux material in evacuated quartz ampoules. The crystal structure and lattice parameters of the $Cu_2Ge(Se_xS_{1-x})_3$ (CGSSe) were determined by X-ray diffraction measurement. Results showed the crystal structure of CGSSe transfers from monoclinic to orthorhombic with increasing the Se content in the powders, which occurs between $0.2 < x < 0.4$. Raman spectroscopy showed that all sulfide related peaks in the solid solutions tend to shift toward smaller wavenumbers and the relative intensity of these peaks was decreasing and selenide related peaks shifted toward higher wavenumbers and decreased. Radiative recombination processes in CGSSe microcrystalline powders were studied by using photoluminescence spectroscopy (PL). All spectra of CGSSe were composed of two asymmetric PL peaks. Peak positions of these bands (#1 and #2) as a function of Se/S concentration show nearly linear dependence with a slope about -0.8 eV. Almost the same slope was detected for band gap values (E_g) determined from room temperature external quantum efficiency measurements. Therefore, the peak position shift with x is related to E_g shift for both PL peaks. Both peaks are related to donor-acceptor pair recombination.

A best performing solar cell was fabricated by using $Cu_2Ge(Se_xS_{1-x})_3$ x = 0.6 powder crystals as absorber material, exhibiting an open-circuit voltage of 537 mV, current density of 15.8 mA/cm^2, fill factor of 37.2% and a conversion efficiency of 3.16%.

1. Introduction

Economic development and the general growth in energy consumption have led to an increased demand for environmentally friendly energy production at lower cost. For these opportunities are sought in the renewable energy sector. New technologies for energy production should provide clean, low cost, environmentally friendly solutions with versatile applications, making solar energy the best solution today. The wide range of multinary compounds have been proposed as emerging inorganic absorber materials for thin film solar cell. Among them, researchers' interest in Cu_2–IV–VI_3 (IV = Ge, Sn; VI = S, Se) ternary compounds and their solid solutions are also growing. For example, Cu_2SnS_3 and $Cu_2(Sn,Ge)S_3$ based solar cells have shown efficiencies 5.1% [1] and 6.73% [2], respectively. Additionally, there are ternary compounds like Cu_2GeS_3 (CGS) and Cu_2GeSe_3 (CGSe), which are not extensively investigated as absorber materials for solar cell application. Germanium is a scarce but not an extremely rare element in the crust of the Earth for example equaling in abundance to molybdenum and exceeding the elements cadmium and antimony. Previously mentioned elements are also widely used in semiconductor industry. CGS and CGSe have many promising properties for photoabsorber material, such as p-type conductivity, high absorption coefficient (10^4 cm^{-1}) and a direct band gap energy [3,4]. Unfortunately, pure sulfide compound has slightly higher bandgap (1.5–1.6 eV) [5,6] and selenide compound have slightly lower (0.78 eV) [7,8] bandgap values reported than it should be for single junction solar cells. Therefore, solid solutions $Cu_2Ge(Se_xS_{1-x})_3$ need to be investigated in order to modify the bandgap energy and find the optimal S/Se ratio for absorber material.

According to several studies, Cu_2GeS_3 exist in different crystal structures, such as orthorhombic, cubic and monoclinic structure, that varies with the synthesis temperature [6,9,10]. Single crystals of CGS grown by chemical vapor deposition method at 620 °C showed

* Corresponding author.
E-mail address: xiaofeng.li@taltech.ee (X. Li).

https://doi.org/10.1016/j.tsf.2021.139053
Received 14 June 2021; Received in revised form 14 December 2021; Accepted 14 December 2021
Available online 16 December 2021

monoclinic crystal structure [9]. Thin films produced by Cu layer annealing in GeS/S vapor at 480 °C showed cubic crystal structure and transition to monoclinic polymorph was observed between 480 and 500 °C [6]. Colloidal nanocrystals (NCs) produced by a hot-injection method showed cubic structure for CGS and by adding Se into the compound, the orthorhombic structure was observed [11]. Although, some researchers have found that CGSe compound crystallize in the monoclinic structure [3,7], mostly it has been observed that pure CGSe crystallize in an orthorhombic structure [3,12,13].

There are only few papers about the defect structure of Cu_2GeS_3, Cu_2GeSe_3 and their solid solutions. Robert et al. [6] reported photoluminescence (PL) studies of the monoclinic Cu_2GeS_3. One PL band with a peak maximum at 1.57 eV was detected, they assigned it to the band to band transition. In the study [12], for Cu_2GeSe_3 compound was detected three PL bands with peaks positions at 0.637 and 0.753 eV which were assigned to free-to-bound recombination from the conduction band to acceptor states and peak position at 0.727 eV was assigned to recombination of an exciton bound to an ionized acceptor. Recently, our group published detailed PL study of $Cu_2Ge(S_{0.4}Se_{0.6})_3$ microcrystals [14]. At LT (low temperature) = 20 K, the donor acceptor pair recombination is dominating for both PL peaks, 1.16 eV and 1.12 eV respectively.

There are only few studies presenting the results about Cu_2GeS_3, Cu_2GeSe_3 or their solid solution based solar cell [6]. The best power conversion efficiency of 2.67% for Cu_2GeS_3 thin film solar cell was achieved by combustion method [4]. In the study [11], the efficiency of 0.2% was presented for solar cells based on $Cu_2Ge(Se_{0.33}S_{0.67})_3$ colloidal NCs.

In the present study, $Cu_2Ge(Se_xS_{1-x})_3$ (x = 0 - 1) high quality microcrystalline powders were synthesized by the molten salt synthesis-growth method with the aim to study structural, compositional and optical properties. The photovoltaic applicability of all $Cu_2Ge(Se_xS_{1-x})_3$ ($x = 0 - 1$) was evaluated by fabricating the monograin layer solar cells.

2. Experimental details

The ternary $Cu_2Ge(Se_xS_{1-x})_3$ (x = 0, 0.2, 0.4, 0.6, 0.8, 1) microcrystalline powders were synthesized from commercially available elements Cu powder (99.999%, Alfa Aesar), Ge powder (99.999%, Alfa Aesar), S powder (99.999%, Alfa Aesar) and Se powder (99.999%, Alfa Aesar) by molten salt method. The alkali salt LiI (99.8%, Alfa Aesar) was used as a molten salt medium (flux material). The used flux salt was added with the mass ratio of $m_{precursors}/m_{flux}$=1:1. The material mixtures were degassed, sealed into quartz ampoules, and then heated from room temperature (RT) to 700 °C at a rate ~0.5 °C/min and maintained at 700 °C for 120 h. Ampoules were cooled down to RT in air, the salt was removed from solid powder particles by leaching with distilled H_2O. Then, the powder was dried in drying oven at 50 °C and sieved into narrow size fractions (38–112 μm) by sieving system Retsch AS 200.

The morphology of synthesized powder crystals was studied by high-resolution scanning electron microscope (HR-SEM Zeiss Merlin). The bulk composition of the synthesized powder crystals was analyzed by energy dispersive X-ray spectroscopy (EDX) by using the Bruker EDX-XFlash 6/30 detector with an accelerating voltage of 20 kV (the measurement error is about 0.5 at%). The crystal structure of studied $Cu_2Ge(Se_xS_{1-x})_3$ microcrystalline powders was characterized by X-ray powder diffraction (XRD) by using a Rigaku Ultima IV diffractometer with monochromatic Cu Kα1 radiation (λ = 1.5406 Å) at 40 kV and 40 mA operating with the silicon strip detector D/teX Ultra. The phase analysis and lattice parameters calculations were made by using software on the Rigaku's system PDXL2. Phase composition of powders was analyzed by room temperature micro-Raman spectroscopy by using a Horiba LabRAM HR800 micro-Raman system equipped with a cooled multichannel CCD detection system in the backscattering configuration with a spectral resolution better than 1 cm^{-1}. A YAG: Nd laser (wavelength λ = 532 nm) was used for excitation. The laser spot size was about 2 μm in diameter. A 0.64 m focal length single grating (600 mm^{-1}) monochromator and the 442 nm line of a He-Cd laser with different power were used for the low temperature PL measurements. For PL signal detection a Hamamatsu InGaAs photomultiplier tube (PMT) or the cooled CCD detector were used. A closed-cycle helium cryostat was employed to measure the PL spectra at temperature T = 20 K. The laser spot size for these measurements was 200 μm in diameter.

The monograin layer solar cells were prepared from chemically and thermally treated powders. Chemical etching and post-annealing were done following the previously developed process in our laboratory [15,16]. For chemical etching, bromine in methanol and KCN solutions were used, and annealing was done in closed quartz ampoules at 400 °C for 60 min. CdS buffer layer was deposited on the post-treated powder crystals by chemical bath deposition method by using vertical rotator in hot-air oven at 60 °C for 30 min. The 360 ° multi-functional vertical rotator provides compact and uniform CdS coverage on CGSSe crystals. An alkali deposition solution contained 0.01 M cadmium iodide (CdI_2) and 1 M thiourea ($SC(NH_2)_2$), 2 M ammonia aqueous solution (NH_4OH) was added to adjust the bath solution pH to 11.6 at room temperature. Monograin membranes were prepared by embedding the CdS covered crystals partway into low shrinkage epoxy resin layer on supporting foil. After curing of epoxy, the membranes were covered with transparent conductive oxide layer (i-ZnO and ZnO:Al) by radio-frequency magnetron sputtering. Finally, back contacts and front collector were made by conductive graphite paste and Ag-paste respectively.

The solar cells were characterized by measuring the current versus voltage (J–V) characteristics with a Keithley 2400 source meter under standard test conditions (AM 1.5, 100 mW cm^{-2}) using a Newport solar simulator. External quantum efficiency (EQE) measurements were performed in the spectral region of 350–1235 nm using a computer controlled SPM-2 prism monochromator. The generated photocurrent was detected at 0 V bias voltage at RT by using a 250 W halogen lamp.

3. Results and discussion

Fig. 1 shows the SEM images of $Cu_2Ge(Se_xS_{1-x})_3$ powder crystals (with fraction size 63–75 μm) synthesized in LiI flux. All formed powders consist of non-aggregated, well-formed single crystals with round edges independent of the S/Se ratio. The median grain size of the powders increased with increasing the selenium content in the $Cu_2Ge(Se_xS_{1-x})_3$ powders. This is also common in quaternary systems, where S/Se in varied [15].

EDX analysis were carried out to confirm the bulk composition of solid solutions. Compositional analysis of bulk was made from polished individual crystals by selecting 8–10 grains for EDX analysis and then average composition is calculated. Table 1 shows the average bulk composition of the $Cu_2Ge(Se_xS_{1-x})_3$ microcrystalline powders. It was found that bulk composition of all powders was slightly Cu-rich and Ge-poor ([Cu]/[Ge]>2), the ratio of [Se]/([S]+[Se]) in synthesized $Cu_2Ge(Se_xS_{1-x})_3$ solid solutions followed nicely the input composition. The ratio of ([S]+[Se])/([Cu]+[Ge]) was approximately 1.0 regardless of the S/Se ratio in material.

Fig. 2a shows the XRD patterns and Fig. 2c shows corresponding lattice parameters of $Cu_2Ge(Se_xS_{1-x})_3$ microcrystalline powders. The major diffraction peaks for pure Cu_2GeS_3 correspond to monoclinic phase (space group *Cc*) (ICDD (PDF-2 01–088–0827) and for pure Cu_2GeSe_3, the characteristic peaks correspond to orthorhombic phase (space group *Imm2*) (PDF-2 01–076–7578). The crystal structure of $Cu_2Ge(Se_xS_{1-x})_3$ transfer from monoclinic to orthorhombic between x = 0.2 to x = 0.4 because the $Cu_2Ge(Se_xS_{1-x})_3$ (x = 0.2) showed monoclinic structure, but further addition of Se in the $Cu_2Ge(Se_xS_{1-x})_3$ (x = 0.4) showed already orthorhombic structure. The position of most intensive diffraction peak shifts from 27.8 deg (for Cu_2GeSe_3) to 29.2 deg (for Cu_2GeS_3) as shown in enlarged view in Fig. 2b.

Using the X-ray diffraction patterns, the values of lattice parameters (*a, b* and *c*) for all powders were calculated and presented in Table 2 and

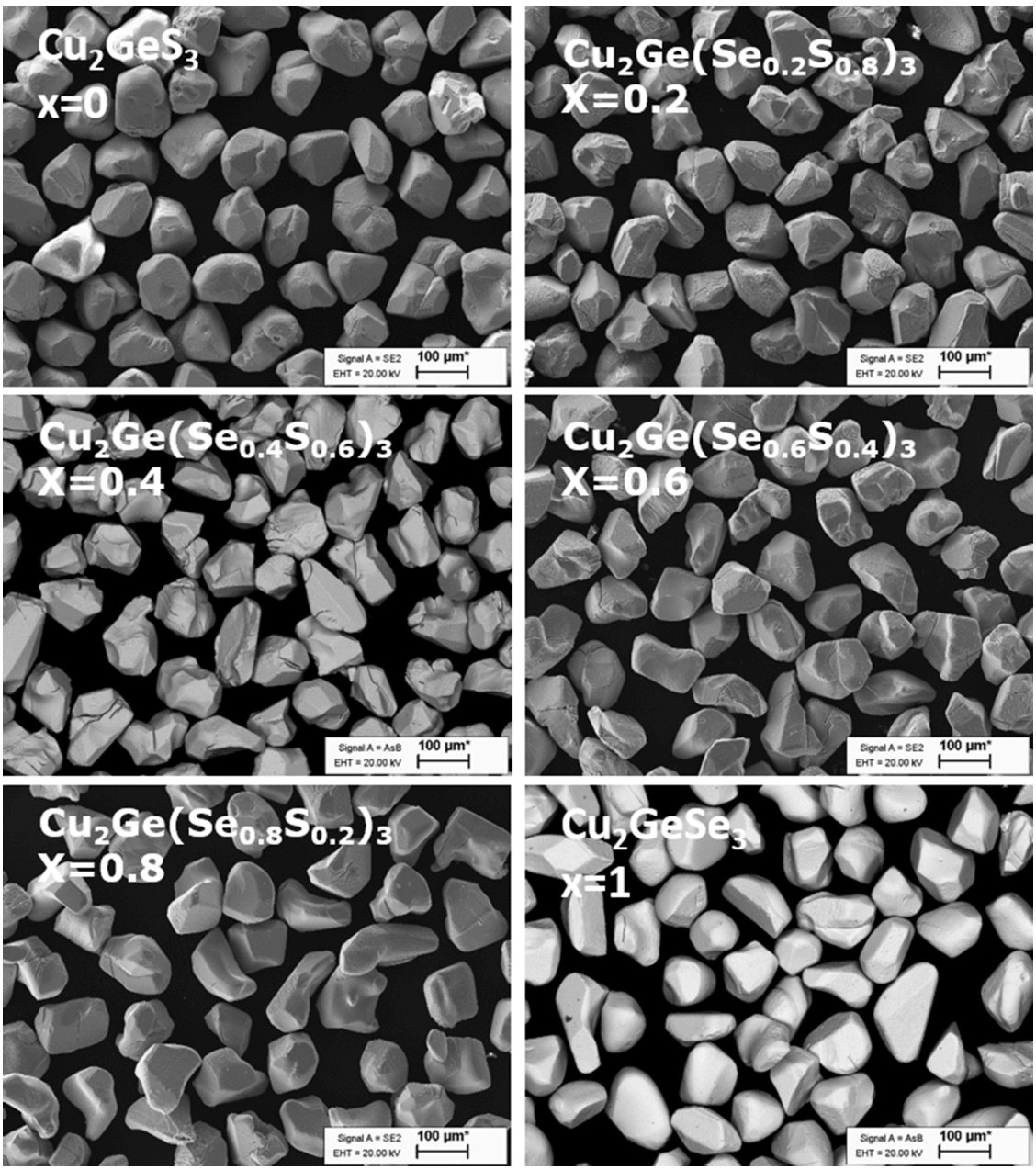

Fig. 1. SEM images of $Cu_2Ge(Se_xS_{1-x})_3$ (x = 0, 0.2, 0.4, 0.6, 0.8, 1) microcrystalline powders.

Table 1
Bulk composition of $Cu_2Ge(Se_xS_{1-x})_3$ (x = 0, 0.2, 0.4, 0.6, 0.8, 1) microcrystalline powders by EDX.

x	Bulk composition of powder crystals by EDX (at%) error~ 0.5 at %				Compositional ratios		
	Cu	Ge	S	Se	[Se]/([S]+[Se])	[Cu]/[Ge]	([S]+[Se])/([Cu]+[Ge])
0.0	33.62	16.28	50.10	–	0.00	2.06	1.00
0.2	33.75	16.51	40.21	9.53	0.19	2.04	0.99
0.4	33.48	16.49	30.01	20.02	0.40	2.03	1.00
0.6	33.48	16.57	19.99	29.96	0.60	2.01	1.00
0.8	33.55	16.24	10.08	40.13	0.80	2.06	1.01
1.0	33.73	16.25	–	50.02	1.00	2.07	1.00

Fig. 2c. Monoclinic Cu_2GeS_3 had lattice parameters a = 6.439 Å, b = 11.316 Å and c = 6.416 Å. Small amount of Se in the $Cu_2Ge(Se_xS_{1-x})_3$ (x = 0.2) increased all the lattice parameters. Additional S replacement by Se in $Cu_2Ge(Se_xS_{1-x})_3$ (x = 0.4 - 1) changed the crystal structure from monoclinic to orthorhombic together with enlargement in the lattice parameter values (a from 11.541 Å to 11.863 Å; b from 3.839 Å to 3.954 Å and c from 5.326 Å to 5.485 Å). This phenomenon is observed upon replacement of sulfur with selenium due to the smaller atom radius of S compared to Se.

Fig. 3 shows the Raman spectra obtained for $Cu_2Ge(Se_xS_{1-x})_3$ solid solutions with different x value. The pure Cu_2GeS_3 crystals show main Raman mode frequencies at 337 and 390 cm^{-1} and minor peaks at 241, 268, 313 and 418 cm^{-1}. All these peaks are assigned to monoclinic CGS phase and are in good correlation to single crystal study [9]. Pure Cu_2GeSe_3 powder crystals showed main Raman peak at 191 cm^{-1} and the additional Raman modes were detected at 184, 220, 268 and 296 cm^{-1}. All these peaks are assigned to orthorhombic Cu_2GeSe_3 phase

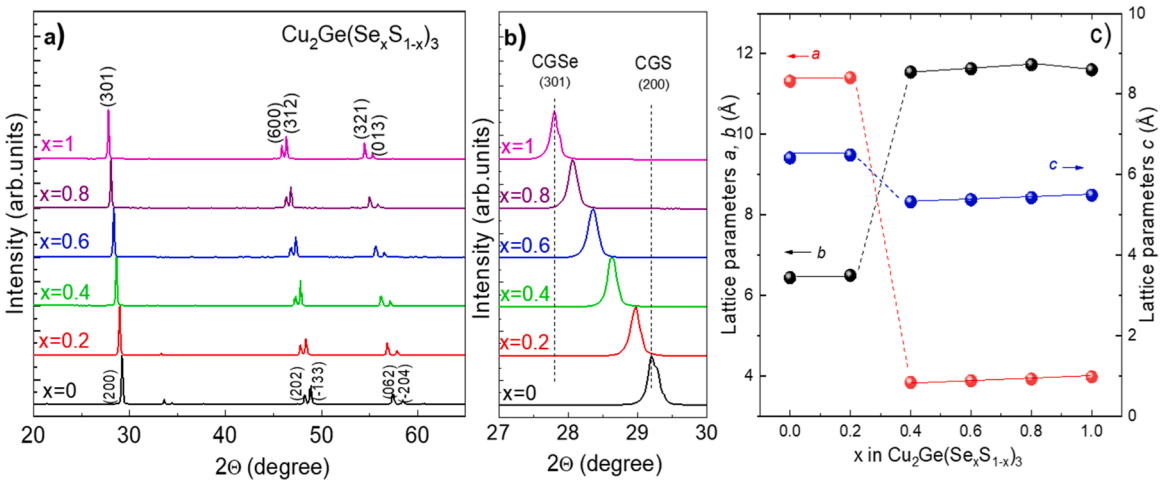

Fig. 2. (a) XRD patterns of $Cu_2Ge(Se_xS_{1-x})_3$ solid solutions (x = 0, 0.2, 0.4, 0.6, 0.8, 1), b) enlarged XRD patterns to view the shift of main peak position and c) lattice parameters.

Table 2
Lattice parameters of $Cu_2Ge(Se_xS_{1-x})_3$ (x = 0, 0.2, 0.4, 0.6, 0.8, 1) microcrystalline powders.

x	*a*, Å	*b*, Å	*c*, Å	V, Å^3	Space group
0.0	6.439	11.316	6.416	443.97	*Cc* [No. 9]-monoclinic
0.2	6.497	11.402	6.486	456.31	*Cc* [No. 9]-monoclinic
0.4	11.541	3.839	5.326	236.32	Imm2 [No. 44]-orthorhombic
0.6	11.626	3.883	5.376	242.70	*Imm2* [No. 44]-orthorhombic
0.8	11.729	3.925	5.428	249.90	*Imm2* [No. 44]-orthorhombic
1.0	11.863	3.954	5.485	257.28	*Imm2* [No. 44]-orthorhombic

[17]. In the solid solutions, all sulfide related peaks tend to shift toward smaller wavenumbers and the relative intensity of these peaks is decreasing and selenide related peaks will shift toward higher wavenumbers. As the x value in the $Cu_2Ge(Se_xS_{1-x})_3$ solid solutions increases, the Raman spectra of $Cu_2Ge(Se_xS_{1-x})_3$ exhibit the two-mode characteristic due to the coexistence of S and Se atoms in powders. This trend is correlated with the increasing structural disorder due to the random distribution of S and Se atoms in the lattice that leads to fluctuations in the masses and force constants in the neighborhood [18]. All peaks belong to the $Cu_2Ge(Se_xS_{1-x})_3$ solid solutions, no other phases were detected.

Fig. 4a shows the normalized photoluminescence spectra of the $Cu_2Ge(Se_xS_{1-x})_3$ solid solutions with different Se/S concentration ratios measured at T = 20 K. All spectra are composed of 2 asymmetric PL peaks. Spectral fitting results with a split-Pearson VII function are shown as colored bands. Peak positions of these bands (#1 and #2) as a function of Se/S concentration show nearly linear dependence with a slope about −0.8 eV. Almost the same slope can be detected for E_g values

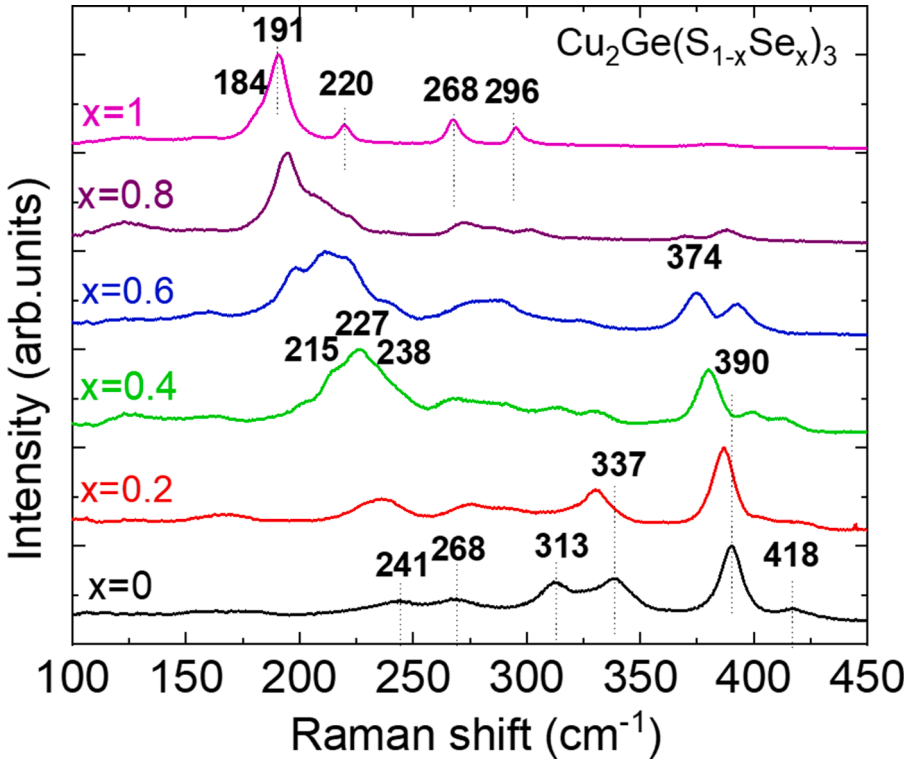

Fig. 3. Room-temperature Raman spectra of $Cu_2Ge(Se_xSe_{1-x})_3$ (x = 0, 0.2, 0.4, 0.6, 0.8, 1) microcrystalline powders.

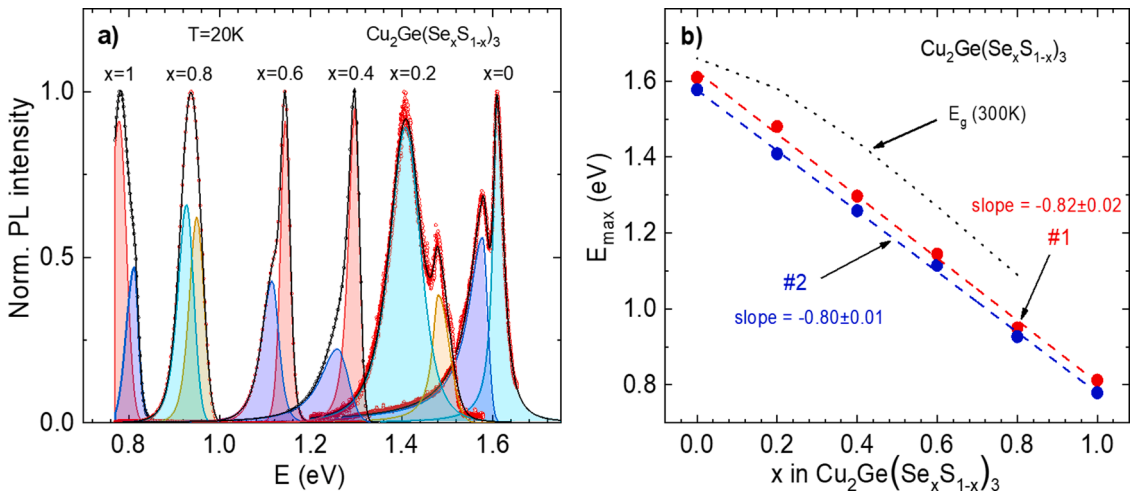

Fig. 4. (a) Normalized low temperature photoluminescence spectra of $Cu_2Ge(Se_xS_{1-x})_3$ solid solutions with different S/Se ratios with fitting using an asymmetric double sigmoidal function, (b) Peak positions of two PL bands as a function of x. Results of linear fitting are shown as dashed lines. Room temperature bandgap energy E_g determined from EQE measurements is given as a dotted line.

determined from room temperature EQE measurements, see Fig 4b. Therefore, the peak position shift with x is related to E_g shift for both PL peaks. The average separation between peak #1 and #2 is around 40 meV. A detailed study of these peaks for $x = 0.6$ was published in [14]. It was shown that both peaks are related to donor-acceptor pair recombination and therefore it is quite likely that the same model holds for the whole range of x values.

The applicability of the $Cu_2Ge(Se_xS_{1-x})_3$ powders as absorber materials were tested in monograin layer solar cell structure. Fig. 5a shows illuminated J–V characteristics and Fig. 5b shows corresponding EQE curves for all studied $Cu_2Ge(Se_xS_{1-x})_3$ based devices. The basic characteristics of solar cells and band gap energy values are presented in Table 3. Cu_2GeSe_3 based solar cell characteristics were excluded because devices did not show any photoresponse.

Open circuit voltage (V_{oc}) of monograin layer solar cells increased from 372 mV to 537 mV by increasing the selenium content in the $Cu_2Ge(Se_xS_{1-x})_3$ from $x = 0$ to $x = 0.6$. Also, current density (J_{sc}) values increased from 5.9 mA/cm^2 to 16.5 mA/cm^2. The monograin layer solar cell with the highest conversion efficiency (η) in this study, which was fabricated from $Cu_2Ge(Se_xS_{1-x})_3$ ($x = 0.6$), demonstrated V_{oc}= 537 mV, J_{sc} = 15.8 mA/cm^2, FF = 37.2%, and η = 3.16%. According to external quantum efficiency (EQE) spectra in Fig. 5b, with the increasing the selenium content in monograin powders, it is obvious to see that the absorption edge shifts to longer wavelengths and the change of spectral response in the long wavelengths. The effective band gap (E_g*) of $Cu_2Ge(Se_xS_{1-x})_3$ solid solutions was evaluated from the linear segment of the low-energy side of the construction (EQE)^2 vs. E curves (inset graph is Fig. 5b). An decrease of E_g* from 1.65 eV to 1.07 eV by increasing Se content in $Cu_2Ge(Se_xS_{1-x})_3$ (x = 0–0.8) powder materials was observed (Table 3).

Table 3
Summary of the main characteristics of $Cu_2Ge(Se_xS_{1-x})_3$ monograin layer solar cells depending on S replacement with Se in absorber materials.

x	V_{oc}, mV	FF,%	J_{sc}, mA/cm^2	η,%	E_g*, eV
0.0	372	39.9	5.9	1.16	1.65
0.2	270	38.1	5.3	0.72	1.57
0.4	415	42.2	16.5	2.90	1.43
0.6	537	37.2	15.8	3.16	1.26
0.8	239	30.6	7.3	0.54	1.07
1	91	25.4	0.7	0.02	–

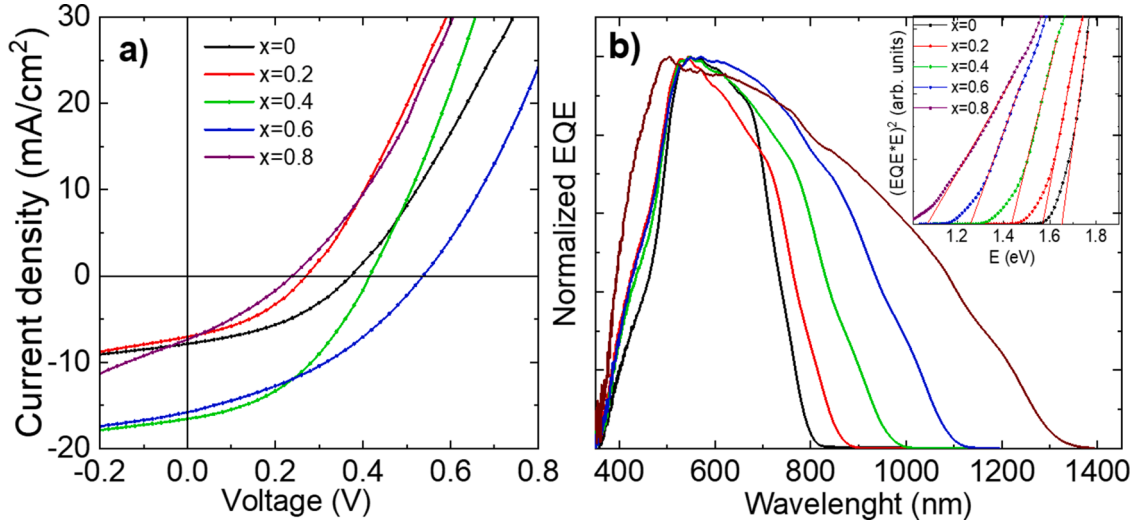

Fig. 5. (a) Light J–V characteristics and b) EQE of $Cu_2Ge(Se_xS_{1-x})_3$ (x = 0, 0.2, 0.4, 0.6, 0.8, 1) monograin layer solar cells. Inset graph shows bandgap extraction by plotting [(EQE*E)^2] vs. E.

Results showed that $Cu_2Ge(Se_xS_{1-x})_3$ ($x = 0.4 - 0.6$) materials have potential as absorber materials in solar cells. Monograin layer solar cells preparation process contain many technological steps which need to be optimized for example optimization of absorber materials composition, selection of buffer layer etc. Therefore, further research is needed to improve the performance of $Cu_2Ge(Se_xS_{1-x})_3$ solar cells.

4. Conclusion

$Cu_2Ge(Se_xS_{1-x})_3$ ($0 \leq x \leq 1$) microcrystalline powders were successfully synthesized in LiI flux by molten salt synthesis–growth method. The compositional analysis by EDX indicated that changing the S/Se ratio in $Cu_2Ge(Se_xS_{1-x})_3$, complete series of solid solutions is formed. All synthesized powders were slightly Cu-rich and Ge-poor. All synthesized powders $Cu_2Ge(Se_xS_{1-x})_3$ consisted of well-formed crystals independent of the S/Se ratio. Structural studies by X-ray diffraction showed that Cu_2GeS_3 crystallize in monoclinic and Cu_2GeSe_3 crystallize in orthorhombic structure. The crystal structure of $Cu_2Ge(Se_xS_{1-x})_3$ transfer from monoclinic to orthorhombic was detected between $x = 0.2$ to $x = 0.4$. Raman and PL studies also confirmed that full series of $Cu_2Ge(Se_xS_{1-x})_3$ is formed. Raman modes of solid solutions followed the bimodal behavior. PL spectra of CGSSe were composed of two asymmetric PL peaks. Peak positions of these bands as a function of Se/S concentration show nearly linear dependence with a slope about −0.8 eV. Almost the same slope was detected for band gap values determined from room temperature EQE measurements. Therefore, the peak position shift with x is related to E_g shift for both PL peaks. Both peaks are related to donor-acceptor pair recombination.

Most promising compounds for solar cell application are $Cu_2Ge(Se_xS_{1-x})_3$ solid solutions with $x = 0.4$–0.6. A best performing solar cell was fabricated by using $Cu_2Ge(Se_xS_{1-x})_3$ $x = 0.6$ powder crystals as absorber material, exhibiting an open-circuit voltage of 537 mV, current density of 15.8 mA/cm^2, fill factor of 37.2% and a conversion efficiency of 3.16%.

CRediT authorship contribution statement

X. Li: Investigation, Validation, Writing – original draft. **K. Timmo:** Supervision, Writing – review & editing. **M. Grossberg:** Writing – review & editing, Funding acquisition. **M. Pilvet:** Investigation. **R. Kaupmees:** Investigation. **J. Krustok:** Investigation, Writing – review & editing. **K. Muska:** Investigation. **V. Mikli:** Investigation, Writing – review & editing. **M. Kauk-Kuusik:** Conceptualization, Supervision, Writing – review & editing, Project administration.

Declaration of Competing Interest

The authors declare that they have no known competing financial interests or personal relationships that could have appeared to influence the work reported in this paper.

Acknowledgments

This study was funded by the Estonian Research Council project PRG1023, by ERDF project “Center of nanomaterials technologies and research (NAMUR+)” (2014–2020.4.01.16–0123), by the European Regional Development Fund “Estonian Center of Excellence project TK141”.

References

[1] A. Kanai, M. Sugiyama, Na induction effects for J–V properties of Cu_2SnS_3 (CTS) solar cells and fabrication of a CTS solar cell over-5.2% efficiency, Sol. Energy Mater. Sol. Cells 231 (2021), 111315, https://doi.org/10.1016/j.solmat.2021.111315.

[2] M. Umehara, S. Tajima, Y. Aoki, Y. Takeda, T. Motohiro, $Cu_2Sn_{1-x}Ge_xS_3$ solar cells fabricated with a graded bandgap structure, Appl. Phys. Express 9 (2016), 072301, https://doi.org/10.7567/APEX.9.072301.

[3] A. Dugarte-Dugarte, N. Ramirez Pineda, L. Nieves, J.A. Henao, G. de Delgado, J. M. Delgado, The crystal structure of Cu_2GeSe_3 and the structure-types of the I_2-IV-VI_3 family of semiconducting compounds, Acta Crystallogr. Sect. B 77 (2021) 158–167, https://doi.org/10.1107/S2052520620016571.

[4] X. Jin, L. Zhang, G. Jiang, W. Liu, C. Zhu, High open-circuit voltage of ternary Cu_2GeS_3 thin film solar cells from combustion synthesized Cu-Ge alloy, Sol. Energy Mater. Sol. Cells (2017), https://doi.org/10.1016/j.solmat.2016.11.001.

[5] H. Araki, K. Chino, K. Kimura, N. Aihara, K. Jimbo, H. Katagiri, Fabrication of Cu_2GeS_3 -based thin film solar cells by sulfurization of Cu/Ge stacked precursors, Jpn. J. Appl. Phys. 53 (2014), https://doi.org/10.7567/JJAP.53.05FW10, 05FW10.

[6] E.V.C. Robert, J. de Wild, D. Colombara, P.J. Dale, M.J. Heben, M.M. Al-Jassim, Crystallographic and optoelectronic properties of the novel thin film absorber Cu_2GeS_3, in: Proceedings of the Thin Films Solar Energy Technology VIII, 2016, 993607, https://doi.org/10.1117/12.2236621.

[7] M. Morihama, T. Maeda, I. Yamauchi, T. Wada, Crystallographic and optical properties of narrow band gap Cu_2GeSe_3 and $Cu_2(Sn_{1-x}Ge_x)Se_3$ solid solution, Jpn. J. Appl. Phys. 53 (2014), https://doi.org/10.7567/jjap.53.05fw06, 05FW06.

[8] G. Marcano, R. Márquez, Variable-range hopping conductivity and magnetoresistance in p-type Cu_2GeSe_3, J. Phys. Chem. Solids 64 (2003) 1725–1727, https://doi.org/10.1016/S0022-3697(03)00195-1.

[9] Y. Matsumoto, N. Aihara, N. Saito, K. Tanaka, Growth of Cu_2GeS_3 bulk single crystals by chemical vapor transport with iodine, Mater. Lett. 194 (2017) 16–19, https://doi.org/10.1016/j.matlet.2017.02.009.

[10] P. Ramasamy, J. Kim, Wurtzite Cu_2GeS_3 nanocrystals: phase- and shape-controlled colloidal synthesis, Chem. Asian J. (2015), https://doi.org/10.1002/asia.201500199.

[11] C. Yang, B. Zhou, S. Miao, C. Yang, B. Cai, W.H. Zhang, X. Xu, $Cu_2Ge(S_{3-x}Se_x)$ colloidal nanocrystals: synthesis, characterization, and composition-dependent band gap engineering, J. Am. Chem. Soc. 135 (2013) 5958–5961, https://doi.org/10.1021/ja400452t.

[12] G. Marcano, G.S. Pérez, C. Rincón, Photoluminescence spectra of Cu_2GeSe_3 orthorhombic semiconductor compound, Phys. Status Solidi 254 (2017), 1700332, https://doi.org/10.1002/pssb.201700332.

[13] D.S. Premkumar, R. Chetty, P. Malar, R.C. Mallik, High temperature XRD of Cu_2GeSe_3, AIP Conf. Proc. 1665 (2015), 120020, https://doi.org/10.1063/1.4918127.

[14] J. Krustok, R. Kaupmees, X. Li, M. Kauk-Kuusik, M. Grossberg, Detailed photoluminescence study of $Cu_2Ge(SSe)_3$ microcrystals, AIP Adv. 11 (2021) 85105, https://doi.org/10.1063/5.0053928.

[15] X. Li, M. Pilvet, K. Timmo, M. Grossberg, V. Mikli, M. Kauk-Kuusik, The effect of S/Se ratio on the properties of $Cu_2CdGe(S_xSe_{1-x})_4$ microcrystalline powders for photovoltaic applications, Sol. Energy (2020), https://doi.org/10.1016/j.solener.2020.09.045.

[16] X. Li, M. Pilvet, K. Timmo, M. Grossberg, M. Danilson, V. Mikli, M. Kauk-Kuusik, Effect of absorber surface modification on the optoelectronic properties of $Cu_2CdGeSe_4$ solar cells, Thin Solid Films (2020), https://doi.org/10.1016/j.tsf.2020.137822.

[17] G. Marcano, C. Rincón, G. Marín, G.E. Delgado, A.J. Mora, J.L. Herrera-Pérez, J. G. Mendoza-Alvarez, P. Rodríguez, Raman scattering and X-ray diffraction study in Cu_2GeSe_3, Solid State Commun. 146 (2008) 65–68, https://doi.org/10.1016/j.ssc.2008.01.018.

[18] M. Grossberg, J. Krustok, J. Raudoja, K. Timmo, M. Altosaar, T. Raadik, Photoluminescence and Raman study of $Cu_2ZnSn(Se_xS_{1-x})_4$ monograins for photovoltaic applications, Thin Solid Films 519 (2011) 7403–7406, https://doi.org/10.1016/j.tsf.2010.12.099.